Mantle Vortex Induced by Downgoing Slab : Experimental Simulation and its Application to Trench-Arc Systems

Mantle Vortex Induced by Downgoing Slab: Experimental Simulation and its Application to Trench-Arc Systems

Hidebumi ITÔ*, Yasuyuki MASUDA* and Osamu KINOSHITA*

(Received June 15, 1983)

In the subduction zones the downgoing slab might induce vortex flow in the lowQ lowV layer. To clarify the dynamics of vortex, experimental simulations are carried out using a viscous fluid and a pattern of streamlines and a velocity distribution in the viscous fluid are obtained for each downgoing angle θ (30°, 45°, 60°, 75° and 90°). From the pattern of streamlines, position of a stagnation point, where the vortex flow wells up to a bottom of the overlying lithosphere, is got as a function of θ. From an analysis of the velocity distribution, a normalized shear strain rate can be calculated. Using it, actual shear stress in the lowQ lowV layer can be evaluated, if the viscosity and the thickness of the lowQ lowV layer and the downgoing velocity of the slab are given.

Thus the authors deduce that the vortex would be induced enough in the lowQ lowV layer with the viscosity 10^{20} poise or so, but a larger vortex extending to 600 km depth would not be induced. The mechanical equilibrium of the landward platelet overlying the vortex is discussed, and the condition for spreading of back-arc basin is derived. When the condition is satisfied, the spreading seems to take place at the stagnation point with the highest possibility. An assumption has been proposed that the back-arc spreading takes place where the landward plate moves away from the trench. However, according to the authors' vortex model, since the induced vortex tends to attach the overlying platelet to the trench, the landward plate moves away leaving the platelet.

The authors' model is applied to the trench-arc systems of Mariana and Tonga-Kermadec where the back-arc basins actively spread now. If the lowQ lowV layer is about 100 km thick, the configulations of stagnation line estimated are fairly well consistent with the topographic features of these basins. Moreover the model is applied for 17 trench-arc systems to calculate the shear force generated by the vortex along the bottom of the platelet. It seems to be not directly concerned with the magnitude of the shear force whether the back-arc spreading takes place or not. It would depend on the force acting horizontally from a trench side.

1. Introduction

In a trench-arc system there is a marked lowQ lowV layer in the mantle under the back-arc, while the descending plate shows contrastively highQ highV (Utsu[1]). The lowQ lowV layer seems to be fluidal compared with the underlying mantle, the overlying lithosphere and the slab. Hence, many investigaters have supposed that the downgoing slab induces a vortex in the lowQ lowV layer as shown schematically in Fig. 5 and have modeled the induced flow to explain the back-arc spreading (McKenzie[2], Sleep and Toksöz[3], Andrews and Sleep[4], Toksöz and Bird[5], Toksöz and Hsui[6], Hsui and Toksöz[7]). A driving force of the vortex is a viscous friction (shear stress) generated at the contact between the slab and the lowQ lowV layer. Toksöz and Hsui[6] have considered that the vortex flow is driven by not only the shear stress but also a buoyancy due to temperature difference. However, in order

* College of Integrated Arts and Sciences.

to induce the vortex flow, the lowQ lowV layer should stick on the slab and the slab should not slip against the lowQ lowV layer. Therefore it must be important to clarify the dynamics of vortex driven by the shear only, as the first step of the study.

The shear stress driving the vortex must be smaller than an adhesive stress (adhesion) between the slab and the lowQ lowV layer. If the shear stress is larger than the adhesion, the slab slips against the lowQ lowV layer and cannot induce a vortex. Could the slab actually induce the vortex in the lowQ lowV layer? If the vortex is induced, it works against the overlying lithosphere to produce a shear stress (viscous friction) at the bottom. How large the shear stress is? To answer these problems an experimental simulation is planed in this paper. Though a resemble simulation was already carried out by Patton as reported in the paper by Toksöz and Bird[5] to get a pattern of streamlines of the vortex, the authors obtain not only the pattern of streamlines but also a velocity distribution in the vortex. Then analysing this velocity distribution, normalized shear strain rates at the upper surface of the slab and the bottom surface of the overlying lithosphere are obtained in order to evaluate actual stresses at the two boundaries.

Based on analyses of the experimental results, the authors get prospects that it would be possible to induce the vortex in the lowQ lowV layer, but it would be difficult to induce a larger vortex extending to 600 km depth where the slab exists, and show conditions under which tensional and compressional stresses develop in a back-arc basin. In the last part of this paper, the authors' vortex model is applied to trench-arc systems, considering the global plate motion.

2. Method of Experiment

To simplify the problem the following assumptions are introduced; (1) the lowQ lowV layer is Newtonian liquid (the Navier-Stokes equation is available), (2) the layer is made of a homogeneous material and (3) the downgoing slab, the overlying lithosphere and the underlying mantle are all regarded to be solid. The assumption (2) is based on that the lowQ lowV layer is in the mantle shallower than about 200 km depth and there is not so marked phase change such as olivine-spinel transition. As the upper surface of the lowQ lowV layer is in contact with the solid lithosphere, there is no free surface. As well known in hydrodynamics, when the free surface is absent and the density is distributed homogeneously, the body force can be neglected in the Navier-Stokes equation. In this case the Reynolds number R must be considered, which is given by

$$R=\rho V_0 L/\eta \tag{1}$$

where ρ and η are density and viscosity, and V_0 and L are the characteristic velocity and length introduced for normalization. In this problem, the velocity of the downgoing slab and the thickness of the lowQ lowV layer are taken to be the characteristic velocity and length. Then the Reynolds number is calculated to be 10^{-19} (dimensionless), provided $\rho=3.4$ g/cm^3, $\eta=10^{20}$ poise, $V_0=10$ cm/y and $L=100$ km. A flow with low Reynolds number ($R\ll 1$) corresponds to a very slow motion and has a characteristic that a pattern of streamlines is independent of the Reynolds

number. Therefore, in the experimental simulation, the Reynolds numbers for the two flows of the lowQ lowV layer and the model are not necessary to be equal and the model must be made to be $R \ll 1$. Moreover the flow with $R \ll 1$ has the characteristics favorable for the experiment, that is, the pattern of streamlines does not change, even if a direction of flow is made to reverse and the flow becomes steady as soon as it starts.

Figure 1 shows a schematic diagram of the experimental apparatus. Viscous fluid modeling the lowQ lowV layer is contained in the case inclined in the upper part of the apparatus, the thickness of the viscous fluid being 40 mm. The case is made of clear acrylic resin. Five cases with inclination angles; 30°, 45°, 60°, 75° and 90° are prepared, these angles corresponding to downgoing angles of the slab. The bed simulating the slab is driven very slowly by an induction motor with a reduction gear. The bed speed is 1.16 mm/sec in maximum (variable). Sodium silicate solution (water glass) is used as the viscous fluid and is poured into the case settled on the bed until the surface level becomes high enough not to affect the vortex flow. Minute air bubbles have been mixed in the water glass in order to visualize the flow pattern. Density and viscosity of the water glass have been measured to be 1.7 g/cm^3 and 2.0×10^3 poise, respectively. Taking bed speed of 1.16 mm/sec, the Reynolds number of the model is 3.9×10^{-4}, which would be sufficiently small for the simulation of very slow motion. In Patton's experiment reported by Toksöz and Bird[5], silicon oil with the kinematic viscosity of 10 stokes and the bed speed of 6 cm/min were employed. The Reynolds number is guessed to be about 0.1 or so, though the thickness of the fluid was not reported.

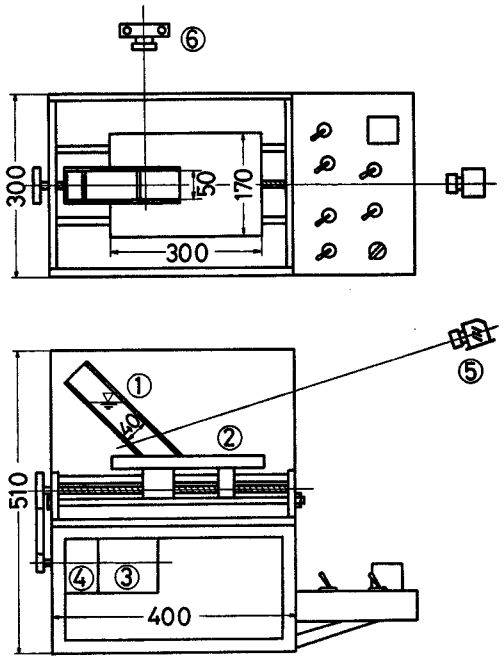

Fig. 1 Experimental apparatus. Dimensions are in mm. 1: case containing viscous fluid, 2: moving bed, 3: motor, 4: reduction gear, 5: light projector, 6: camera.

The above model is illuminated perpendicular to the camera axis (ref. Fig. 1) by the light about 2 mm thick through a narrow slit in a dark room, and in this way the minute bubble tracers distributed only in the illuminated section can be observed. It has been confirmed that two dimensional flow is held in the model except the boundary layer of side wall of the case by means that the illuminated section is moved before and behind along the camera axis. It is important in this experiment to obtain the flow pattern of streamlines and the velocity distribution of flow. The trajectories of sparkling minute bubbles are photographed in 2 minutes exposure to get the flow patterns. Velocity distribution is photographed by means of switching on and off the light. The switching intervals are taken 4 sorts of 5, 10, 20 and 30 seconds since the velocity of the vortex flow depends largely on the position. The observations of the flow pattern and the velocity distribution are carried out for five sorts of the model.

3. Results of the Experiment

The flow patterns obtained for five configulations are shown in Fig. 2. In each photograph the upper and lower boundaries are fixed, and the right inclined one moves very slowly. The operational speed is 1.16 mm/sec. As seen in Fig. 2 streamlines of the first vortex are shown very sharply and delicately, but the second vortex in the rear of the first one has not been photographed except in the case of the angle 45°. The second vortex is extremely weak compared with the first one. In order to observe the second vortex, longer exposure is required to get longer paths of tracers. The patterns in Fig. 2 are obtained by advancing the bed to the direction of slab motion. Patterns obtained when the bed advances reversely are not shown here. Each of them is almost the same as one in Fig. 2 for the first vortex.

Streamlines for 90° have been calculated numerically by Kawaguti[8], where the Navier-Stokes equation has been solved by the finite difference method. The streamlines solved subject to very low Reynolds number agree well with those on the case of 90° in Fig. 2. This means that the water glass under the condition $R=3.9\times10^{-4}$ mentioned previously behaves as Newtonian liquid.

Figure 3 shows the positions of the vortex centers for various downgoing angles. In this figure, the vertical and horizontal scales are normalized by the thickness L of the fluid layer. It is remarkable that the length of the perpendicular from the vortex center to the slab surface seems to have always a constant value of $0.23\times L$. This shows that the velocity distribution of flow across the perpendicular resembles closely for every downgoing angles.

Figure 4 shows the relationship between the downgoing angle θ and the normalized distance S/L, where S is the distance from the upper corner to the stagnation point (ref. Fig. 5b). The dividing point of the first vortex and the second one is called the stagnation point. S/L decreases gradually when θ increases. This relationship is used in the later section.

The velocity distribution in the vortex flow has been got by the way mentioned in the last part of the preceding section, although the photographes are not shown here (ref. Kinoshita et al.[9]). The velocity distribution is also necessary in the later discussions.

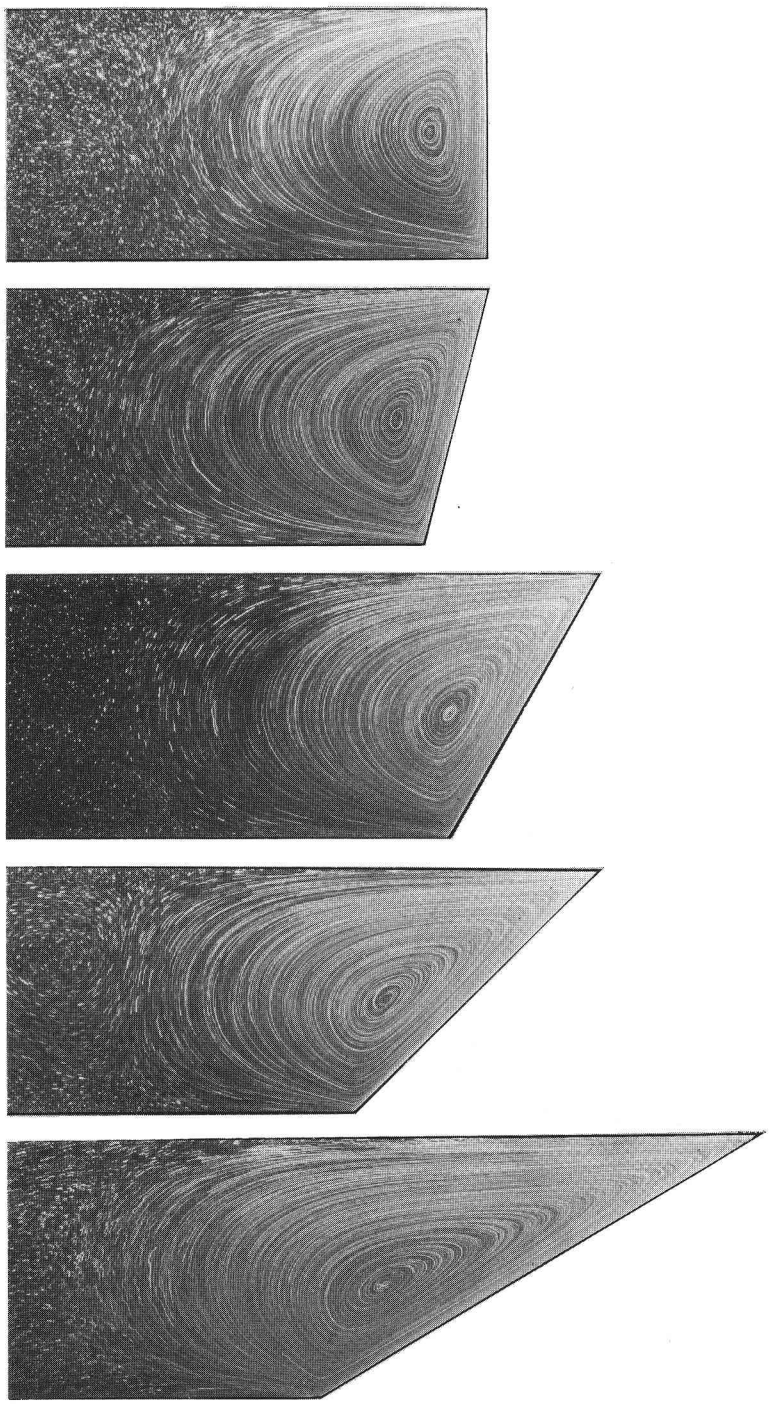

Fig. 2 Flow patterns obtained in experimental simulations. Inclinations of right boundaries simulating a downgoing slab surface are 90°, 75°, 60°, 45° and 30°.

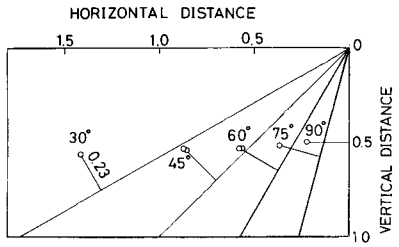

Fig. 3 Positions of the vortex centers for various downgoing angles. Each of inclined lines shows the slab surface. Vertical and horizontal scales are normalized by the thickness of fluid layer. Two vortex centers have been obtained for two cases that the slab advances normally and reversely, though they do not coincide with each other for 45° and 60°.

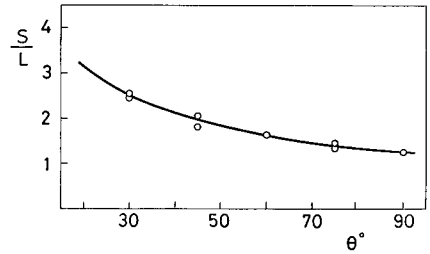

Fig. 4 Relation between the downgoing angle θ and the position of stagnation point S measured from the upper corner. L is the thickness of fluid layer.

4. Shear Stress along the Downgoing Slab and Condition to Induce the Vortex Flow

When the downgoing slab induces the vortex, a shear stress is produced along the contact plane with the lowQ lowV layer. The shear stress τ' is expressed by

$$\tau' = \eta \left(\frac{\partial u'}{\partial y'} \right)_0 \tag{2}$$

where the coordinate axes x' and y' are taken as shown in Fig. 5(a), u' is x'-component of the flow velocity and $(\partial u'/\partial y')_0$ is shear strain rate at the slab surface (at $y'=0$). Introducing the normalized variables; $U'=u'/V_0$, $X'=x'/L$ and $Y'=y'/L$, the normalized shear strain rate is given by

$$\left(\frac{\partial U'}{\partial Y'} \right)_0 = \frac{L}{V_0} \left(\frac{\partial u'}{\partial y'} \right)_0 \tag{3}$$

and the actual shear stress τ' can be calculated by the equation;

$$\tau' = \frac{\eta V_0}{L} \left(\frac{\partial U'}{\partial Y'} \right)_0 \tag{4}$$

The normalized ones must be equal for both the model and the lowQ lowV layer. Since the velocity distribution has been got diagramatically for the model as mentioned above, $(\partial u'/\partial y')_0$ is also obtained, but it is unable to be measured near the upper corner. Thus, $(\partial U'/\partial Y')_0$ is got from eq. (3) (with $L=4$ cm and $V_0=1.16$ mm/sec) as shown in Fig. 6. Each of the curves shows U-shaped or deformed U-shaped, and the normalized strain rate increases steeply toward the upper corner ($X'=0$). The mean values of $(\partial U'/\partial Y')_0$ are calculated to be 12.5 for $\theta=30°$, 11.1 for 45°, 10.7 for 60°, 10.6 for 75° and 11.0 for 90°.

The shear stress τ' depends on η, V_0 and L, but we do not know their reliable values especially for η. The viscosity of the asthenosphere has been estimated to be 10^{22} to 10^{21} poise from the post glacial uplift of Fenno-Scandia and from the

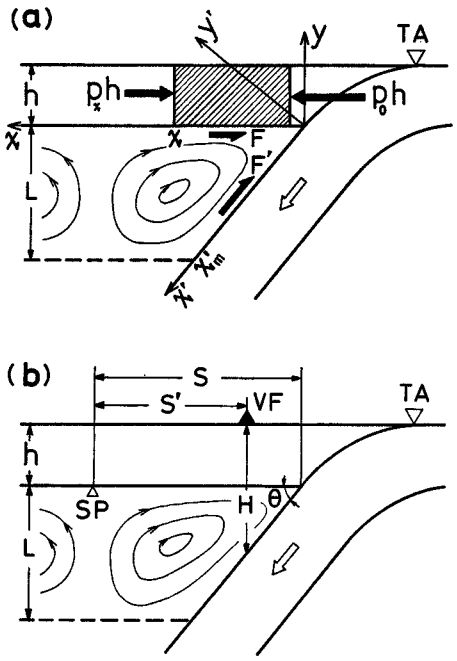

Fig. 5 Schematic diagram of vortex induced by a downgoing slab. (a): figure to explain mechanical relations, (b): figure to explain the relation between S, S', H, h and θ. TA: trench axis, VF: volcanic front, SP: stagnation point.

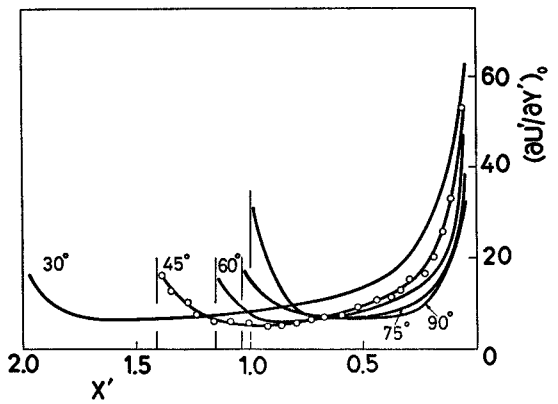

Fig. 6 Distribution of normalized shear strain rate at a boundary simulating the slab surface. Measured values are shown by circles only for the curve of $\theta=45°$. Note that each curve increases steeply toward $X'=0$.

Pleistocene lake uplift in Utah, USA. McConnell[10] has obtained so smaller values as 10^{20} and 10^{19} poise for his layered model 7 and 9, respectively. Since the viscosity of the lowQ lowV layer seems to be smaller than the average viscosity of the asthenosphere, the authors employ $\eta=10^{20}$ poise in the following discussion. Moreover, provided $L=100$ km and $V_0=10$ cm/y, $(\partial U'/\partial Y')_0=1$ corresponds to $\tau'=3.17$ bar, and therefore the average shear stress ranges from 40 to 34 bar. As noted previously, the shear stress is necessary to be smaller than the adhesion between the

slab and the lowQ lowV layer in order to induce the vortex, otherwise the slab slips against the lowQ lowV layer. We have not detailed knowledge about the adhesion. However, the following fact might give one measure for the adhesion. Referring to the study by Geller[11], thrust type earthquakes occuring near the trench show the stress drop ranging from 17 to 64 bar (30 bar in average), which suggests that actual shear strength, that is, the adhesion between the slab and the lithosphere of island arcs might be less than 100 bar or so. Although the numerical value of adhesion between the slab and the lowQ lowV layer is not still certain, if it is 100 bar or so, the following argument will be possible based on Fig. 6.

The shear stress may be not so large compared with the adhesion except near the upper corner, and the vortex would develop enough in the lowQ lowV layer, unless η is extremely larger than 10^{20} poise. Near the upper corner the normalized shear strain rate is very large as seen in Fig. 6. Because of the large shear stress, the slab might slip and the flow would not occur there.

Total shear force F' and total energy E per unit time to induce the vortex in the lowQ lowV layer are given by

$$F'=\eta\int_0^{x_m'}\left(\frac{\partial u'}{\partial y'}\right)_0 dx'=\eta V_0\int_0^{X_m'}\left(\frac{\partial U'}{\partial Y'}\right)_0 dX' \tag{5}$$

and

$$E=\eta V_0^2\int_0^{X_m'}\left(\frac{\partial U'}{\partial Y'}\right)_0 dX' \tag{6}$$

where x_m' is shown in Fig. 5(a) and $X_m'=x_m'/L$. F' and E are not concerned with the thickness L of the lowQ lowV layer. The curves of the integral of $(\partial U'/\partial Y')_0$ with respect to X' are shown in Fig. 7, where the integration is done except near the upper corner, and the magnitude of the integral in eqs. (5) and (6) is known for each angle. The total shear force and the total energy decrease clearly with the downgoing angle. This implies that the larger force and energy are required when the slab descends with the lower downgoing angle.

On the other hand, as the descending slab exists not only in the lowQ lowV

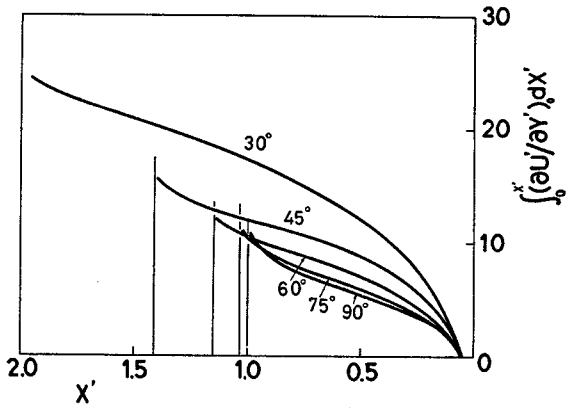

Fig. 7 Values of integral of $(\partial U'/\partial Y')_0$ in Fig. 6 with respect to X'. Note that maximum value for each curve decreases with angle θ.

layer but also down to 600 km depth, it will be examined whether a larger vortex extending to the 600 km depth is induced or not. Supposing $\eta=10^{22}$ poise, $L=600$ km and $V_0=10$ cm/y, $(\partial U'/\partial Y')_0=1$ corresponds to $\tau'=52.8$ bar. If the adhesion between the slab and the upper mantle is 100 bar or so as well as that between the slab and the lowQ lowV layer, it is supposed that the slab is difficult to descend to 600 km depth inducing the larger vortex. Moreover, the total shear force and the total energy to induce such vortex are 100 times as large as those for the lowQ lowV layer with 10^{20} poise. The slab would penetrate into the upper mantle forming a lubricant layer such as low viscous fluid layer along the upper surface of itself.

5. Stress Developed in the Overlying Lithosphere

Vortex flow induced by the downgoing slab generates a shear stress along the bottom of the overlying lithosphere (Fig. 5a). Doing the same treatment as in the preceding section, the shear stress τ is given by

$$\tau=\eta\left(\frac{\partial u}{\partial y}\right)_0=\frac{\eta V_0}{L}\left(\frac{\partial U}{\partial Y}\right)_0 \tag{7}$$

where the coordinate axes x and y are taken as shown in Fig. 5(a), u is a horizontal component of flow velocity and the normalized variables U, X and Y are used as the same way. Figure 8 shows the relationship between $(\partial U/\partial Y)_0$ and X obtained by the experiment for the first vortex. It is clear that the shear stress decreases with a distance x from the upper corner of the lowQ lowV layer and reaches to zero at the stagnation point of the vortex. Provided $\eta=10^{20}$ poise, $L=100$ km and $V_0=10$ cm/y, $(\partial U/\partial Y)_0=1$ corresponds to $\tau=3.17$ bar. As $(\partial U/\partial Y)_0$ is less than 10 or so excepting near the upper corner (Fig. 8), the shear stress τ is less than 30 bar or so.

The shadowed portion of the overlying lithosphere (Fig. 5a) must be in a mechanical equilibrium as expressed by the equation;

$$(p_0-p_x)h=F \quad \text{or} \quad p_x=p_0-F/h \tag{8}$$

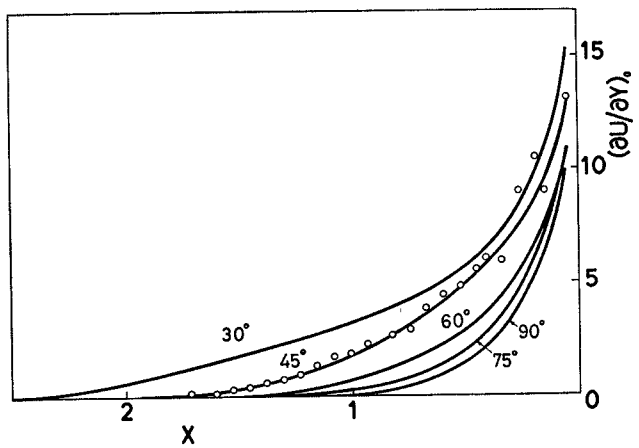

Fig. 8 Distribution of normalized shear strain rate at a boundary simulating the bottom surface of the overlying lithosphere. Measured values are shown by circles only for the curve of $\theta=45°$.

where h is a thickness of the overlying lithosphere, $p_o h$ a tectonic force caused by a motion of the oceanic lithosphere and $p_x h$ a tectonic force acting at a place x. F is the shear force induced by the vortex and given by

$$F=\eta\int_o^x\left(\frac{\partial u}{\partial y}\right)_0 dx=\eta V_0\int_o^X\left(\frac{\partial U}{\partial Y}\right)_0 dX=\eta V_0 I(\theta, X) \tag{9}$$

For further description, the function $I(\theta, X)$ has been introduced;

$$I(\theta, X)=\int_o^X\left(\frac{\partial U}{\partial Y}\right)_0 dX \tag{10}$$

F is also not concerned with L. Figure 9 shows the relationship between $I(\theta, X)$ and X. It is clearly seen that the shear force F increases with x and reaches to a maximum at the stagnation point of the vortex. Therefore, p_x decreases with x (eq. 8) and becomes to be negative in the case of $p_o<F/h$. The negative p_x means a tensional stress, which may cause a possible spreading of the overlying lithosphere.

The magnitude of F/h in eq. (8) can be calculated using Fig. 9, if the values of h, V_0 and η are given. Assuming $h=50$ km, $\eta=10^{20}$ poise and $V_0=10$ cm/y, $I(\theta, X)=1$ corresponds to $F/h=6.35$ bar, and therefore F_s/h, the value at the stagnation point, is calculated to be 14.6 bar for the downgoing angle 90° and 50.8 bar for 30°. If p_o is smaller than these values, p_x is able to become negative and back-arc spreading may occur. This suggests that the back-arc spreading takes place where the tectonic stress p_o acting horizontally is rather small.

As the tensional stress p_x becomes to be maximum at the stagnation point, the spreading seems to take place there with the highest possibility. The condition whether or not the back-arc spreading takes place is given by

$$\left.\begin{aligned} &p_o<F_s/h=\frac{\eta V_0}{h}I(\theta, S/L) && \text{for spreading}\\ &p_o>F_s/h && \text{for not spreading}\end{aligned}\right\} \tag{11}$$

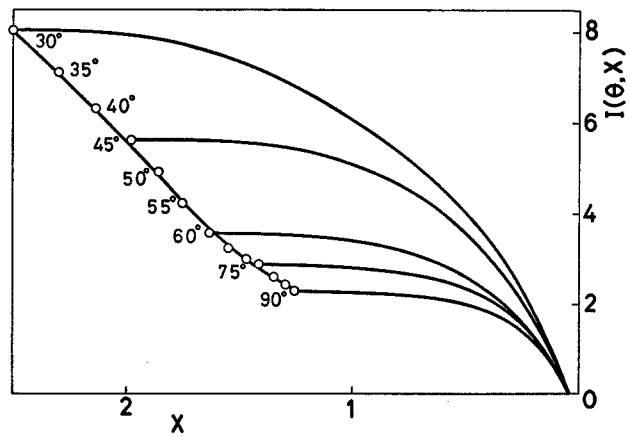

Fig. 9 Values of $I(\theta, X)$ for $\theta=30°$, 45°, 60°, 75° and 90°. $I(\theta, X)$ is defined by eq. (10). The left curve attached by numerical values of θ shows relation between $I(\theta, S/L)$ and θ.

Here the global plate motions are considered. Chase[12] and Uyeda and Kanamori[13] have discussed that the back-arc opening takes place where the landward plate moves away from the trench. According to the authors' vortex model, the platelet overlying the first vortex tends to be attached to the trench by the force F. Therefore, the major part of landward plate moves away leaving the platelet and consequently the back-arc spreading takes place near the stagnation point. The authors consider that the boundary of the motions between the oceanic plate and the landward plate is represented by the stagnation line of vortex, the stagnation point coming out as a line on the earth's surface.

An absolute velocity of the trench motion is important in this consideration, but it is unknown. If the velocity is the same with an absolute velocity of the landward plate, the oceanic plate descends with a relative velocity of the oceanic and the landward plates, and the vortex develops in the direction of the relative motion. If the absolute velocity of the trench is zero, the oceanic plate descends with its absolute velocity and induces the vortex in its direction. Whenever the trench moves more slowly than the landward plate, it moves away from the platelet and the back-arc spreading results. As the trench motions are unknown, the motion of downgoing slab cannot be decided. Therefore the authors consider it for extreme two cases of relative and absolute motions in the next section.

6. Application of the Model to Trench-Arc Systems

In this section, the model on the mantle vortex described above is applied to the island arc systems. Figure 5(b) shows the section of an island arc area in the direction of plate movement. The slab is considered to descend to the direction of the plate movement, not to that perpendicular to the trench axis. Accordingly, the vortex may be induced in the section illustrated in Fig. 5(b). As indicated in the figure, H is the depth of the descending slab surface at the volcanic front and S' the distance from it to the stagnation point. Then S' is given by the relation;

$$S'=S-(H-h)\cot\theta \tag{12}$$

The upper surface of descending slab is approximated by the seismic plane of deep focus earthquakes. A dip angle θ^* of the seismic plane around 50 to 200 km depth is measured from the seismic data of literature as given in Table 1. The depth H is also shown in the table. The dip angle θ^* of Table 1 is different from the downgoing angle θ of Fig. 5(b) and eq. (12). The angle θ is calculated by the equation;

$$\tan\theta=\tan\theta^*\cos\alpha \tag{13}$$

where α is an angle between the direction perpendicular to the trench axis and that of the movement of oceanic plate.

The direction and rate for relative and absolute plate movements are determined on the basis of the MR-2 and AM 1–2 models of Minster and Jordan[14] and the model by Seno[15]. The authors decide the directions at several points on the trench for each arc and get α and θ as given in Table 1. In order to calculate S' in eq. (12) the thickness h of the landward plate is assumed to be 50 km. Because the thickness

Table 1 Data used in calculations for positions S' of stagnation points and for stresses F_s/h caused by the induced vortex. See eqs. (12) and (13) for S', H, θ, θ^* and α, and eq. (11) for V_0, $I(\theta, S/L)$ and F_s/h. θ^* and H are from Isacks and Barazangi[29].

		Relative plate motion						Absolute plate motion					
	Position on the trench axis	Direction of plate motion	α (°)	θ (°)	V_0 (cm/y)	$I(\theta, S/L)$	F_s/h (bar)	Direction of plate motion	α (°)	θ (°)	V_0 (cm/y)	$I(\theta, S/L)$	F_s/h (bar)
Mariana	147.6°E 19.4°N	N60°W	43	46.3	4.9	5.25	16.3	N69°W	34	49.9	10.8	4.75	32.3
$\theta^*=55°$	147.9°E 17.8°N	N58°W	32	50.6	4.2	4.65	12.4	N69°W	21	53.3	10.8	4.31	29.3
$H=100$km	147.8°E 15.4°N	N56°W	21	53.2	3.9	4.33	10.7	N69°W	8	54.8	10.7	4.15	28.0
	146.9°E 13.6°N	N56°W	0	54.3	3.2	4.14	8.4	N69°W	13	54.3	10.7	4.22	28.4
Tonga	172.6°W 18.3°S	N82°W	8	47.7	10.0	5.08	32.0	N61°W	14	47.2	10.5	5.13	33.9
$\theta^*=48°$	173.0°W 20.0°S	N82°W	12	47.4	9.3	5.09	29.8	N61°W	9	47.6	10.3	5.07	32.9
$H=95$km	174.2°W 22.5°S	N82°W	17	46.7	8.9	5.20	29.2	N61°W	5	47.9	10.2	5.03	32.3
Kermadec	176.1°W 29.5°S	N82°W	5	64.9	7.7	3.31	16.1	N59°W	19	63.8	9.7	3.37	20.6
$\theta^*=65°$	176.5°W 30.4°S	N82°W	14	64.3	7.4	3.35	15.7	N59°W	11	64.5	9.5	3.33	19.9
$H=100$km	177.1°W 31.5°S	N82°W	15	64.2	6.7	3.35	14.1	N58°W	9	64.7	9.3	3.32	19.5

L of the lowQ lowV layer is not certain for individual arcs, S is got for various values of L from the relationship between S/L and θ in Fig. 4.

The authors have mentioned previously that the slab might slip and the flow would not occur near the upper corner in the lowQ lowV layer. However, it has been confirmed by preliminary experiments that the position of the stagnation point is almost unchanged even if the induced flow does not occur near the upper corner.

The Mariana trough is crescent shaped and 200 km wide at the center of the arc, lying between the Mariana Ridge with a volcanic chain and the West Mariana Ridge (Fig. 10). The geological and geophysical surveys have been done by Karig[16], Karig et al.[17] and others. The zone of youngest crust by Karig et al.[17] is additionally shown in Fig. 10. The back-arc spreading is supposed to occur along

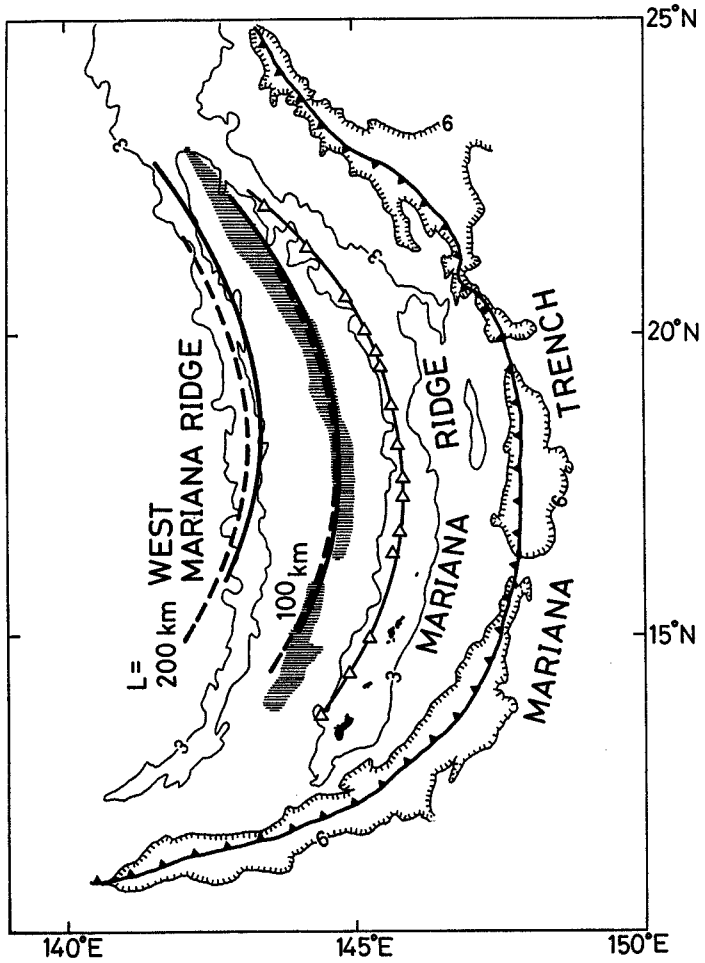

Fig. 10 Map of the Mariana trench-arc system, showing positions of stagnation line calculated by the authors' vortex model. The stagnation lines are drawn assuming L=100 and 200 km by heavy lines; solid lines are for the relative plate motion and broken lines for the absolute one. The topography has been constructed after Karig[16] (his Figs. 1 and 2); depths are in km and triangles recent volcanoes. Horizontal ruling area shows the zone of youngest crust by Karig et al.[17] (their Fig. 3).

the zone, which corresponds topographically to the axial high lying halfway between the scarp systems bounding the trough.

The positions of the stagnation points are calculated for the two cases of the relative and absolute plate motions by eq. (12) using the data of θ and H in Table 1. The results of calculation are shown in Fig. 10 by the lines (stagnation lines) for $L=100$ km and 200 km. As seen in the figure, the stagnation lines for both the relative plate motion (solid lines) and the absolute one (broken lines), especially those of $L=100$ km, are similarly situated. The configulation of the zone of youngest crust seems to coincide well with the stagnation line of $L=100$ km. The thickness of the lowQ lowV layer is estimated to be about 100 km beneath the Mariana arc region. The stagnation line for $L=200$ km is useful for evaluating an extent of the coincidence. The volcanic chain and the West Mariana Ridge have apparently different curvatures to each other, and the trough is open at the southern end and is close at the northern end. In order to explain this morphorogical situation, Le Pichon[18], Brancey and Ogden[19] and Karig et al.[17] have proposed possible opening

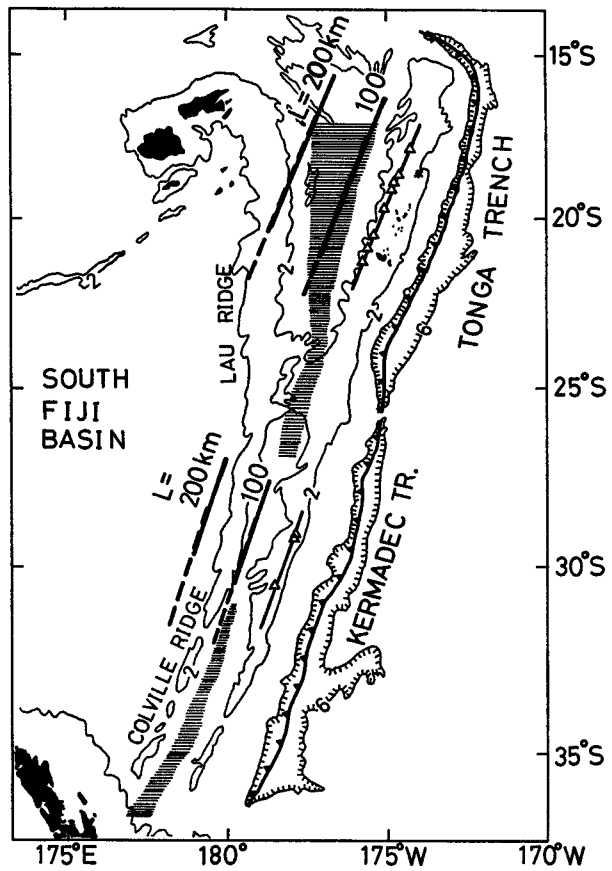

Fig. 11 Map of the Tonga-Kermadec trench-arc system, showing positions of stagnation line. The topography has been constructed after Karig[20] (his Fig. 3) and recent volcanoes based on Katsui[22]. Horizontal ruling shows areas where sediment thickness is zero according to Karig[20] (his Fig. 9).

models. However, the model presented here seems to interprete it well.

The Lau-Havre basin, which is between the Tonga-Kermadec ridge and the Lau-Colville ridge, is considered to be now opening (Karig[20),21)]) (Fig. 11). The stagnation lines calculated for $L=100$ km and 200 km are illustrated in Fig. 11. There is no difference in the positions of stagnation lines for both the relative plate motion and the absolute one. The thickness L for the Tonga arc is estimated to be about 100 km and that for the Kermadec arc is to be slightly less than 100 km.

On the other hand, the values of F_s/h for the Mariana and Tonga-Kermadec arcs are calculated by eq. (11) assuming $\eta=10^{20}$ poise and $h=50$ km, and are shown in Table 1 and in Fig. 12 for the two cases of the relative and the absolute plate motions. V_0 and $I(\theta, S/L)$ used in the calculation are also given in the table. The values of F_s/h for the relative plate motion are apparently or slightly less than those for the absolute plate motion. Especially for the Mariana arc the values of F_s/h

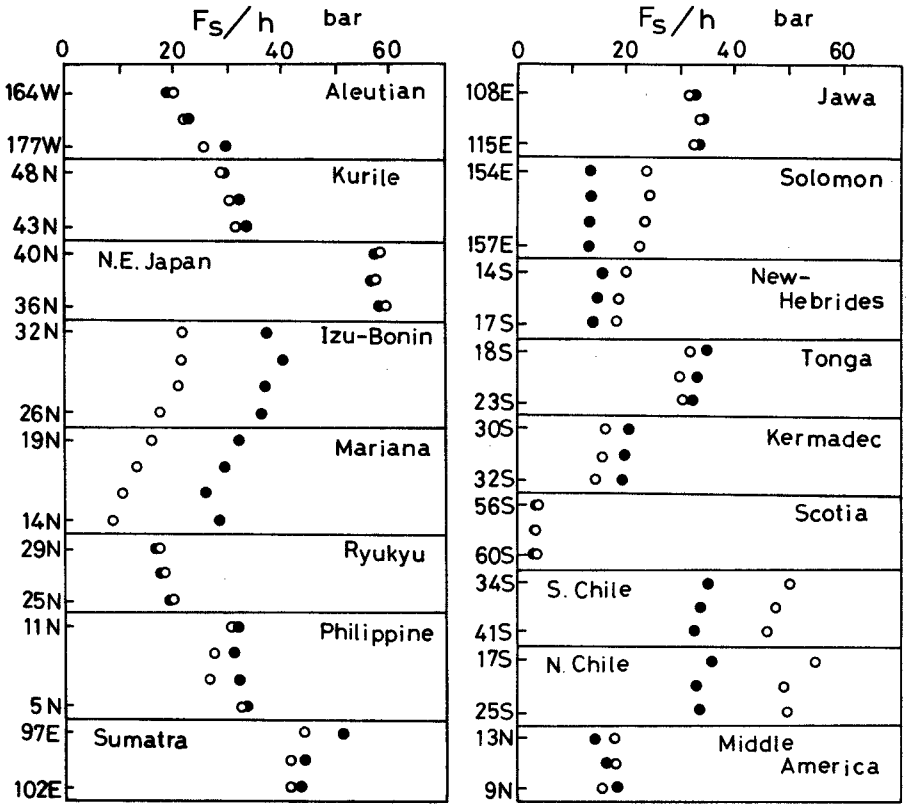

Fig. 12 The stress F_s/h in the overlying lithosphere caused by the induced vortex for various trench-arc systems. The open circles are for the relative plate motion, and the solid circles for the absolute one. Data sources of θ^* (dip of the slab) necessary for calculation of F_s/h are as follows, Aleutian and Kurile: Engdahl et al.[23)], Northeast Japan: Yoshii[24)], Izu-Bonin, Mariana and Ryukyu: Katsumata and Sykes[25)], Philippine, Sumatra and Jawa: Hamilton[26)], Solomon: Denham[27)], New Hebrides: Dubois[28)], Tonga, Kermadec, South Chile and North Chile: Isacks and Barazangi[29)], Scotia: Santo[30)], Middle America: Dewey and Algermissen[31)].

for the relative plate motion are considerably small (8.4 to 16.3 bar). If the relative plate motion is applicable, the value of p_o for Mariana must be less than 8.4 bar.

Similar calculation are done for the other trench-arc systems, though the used parameters V_0, θ and $I(\theta, S/L)$ are not given here. In the calculations the thickness h is assumed to be 50 km evenly for all arcs, although the value for the continental arcs represented by Chile may be larger. The values of F_s/h for various arc systems are shown in Fig. 12. They are ranging from about 3 bar to about 59 bar, and their mean is 27.5 bar for the relative plate motion and is 28.3 bar for the absolute one. Maximum value of F_s/h is found in Northeast Japan arc, where no back-arc spreading occurs now. Conversely, at Scotia arc, where the back-arc spreading is regarded to now actively occur (Uyeda and Kanamori[13]), the value of F_s/h is minimum. This means that the magnitude of force caused by the induced vortex, F_s/h, is not directly concerned with the back-arc spreading. It may be concerned with the value of p_o (ref. eq. 11), and the value of p_o is possibly related to the motion of landward plate.

7. Conclusion

Under the assumption that the downgoing slab induces the vortex flow in the lowQ lowV layer, the experimental simulation has been carried out and the streamlines and the velocity distribution have been obtained for the downgoing angles 30°, 45°, 60°, 75° and 90°. Based on the analyses of the experimental results, the following points are emphasized.

1) The normalized shear strain rates of vortex flow at the slab surface have been got in Fig. 6. From this figure the shear stress τ' and the total shear force F' at the slab surface and the energy E per unit time to induce the vortex are estimated by eqs. (4), (5) and (6), respectively. Estimating these numerical values, the authors have deduced that the vortex would be induced enough in the lowQ lowV layer with the viscosity 10^{20} poise or so, but a larger vortex throughout the upper mantle would not. Perhaps the slab would penetrate into the mantle underlying the lowQ lowV layer by the other way.

2) The normalized shear strain rates at the bottom of the overlying landward lithosphere have been also obtained as shown in Fig. 8 in order to estimate numerical values of the shear stress τ (eq. 7) and the shear force F (eq. 9) along the bottom surface. The mechanical equilibrium on the landward plate is shown in Fig. 5(a), where the three forces p_oh, p_xh and F are concerned. Thus the condition of back-arc spreading has been derived in eq. (11).

3) The back-arc spreading has been considered so far to take place where the landward plate moves away from the trench (Chase[12], Uyeda and Kanamori[13]). However, since the induced first vortex tends to attach the overlying platelet to the trench, the authors have proposed the new idea that the major landward plate moves away leaving the platelet and therefore the back-arc spreading takes place near the stagnation line.

4) The authors' vortex model has been applied to the trench-arc systems of Mariana and Tonga-Kermadec where the back-arc basins appear to actively open.

If the lowQ lowV layer exists from 50 to 150 km depths (about 100 km thick), the configulations of stagnation line are fairly well consistent with the topographic features of these basins.

5) Moreover the authors' model has been applied for 17 trench-arc systems to calculate F_s/h (ref. eq. 11). From the results (Fig. 12) the back-arc spreading seems to be not directly related to F_s/h. It would depend on p_o whether the back-arc spreading takes place or not, p_o being probably related to the coupling between the oceanic and landward plates.

For further discussion, the authors will complete the experiment that the flow does not occur near the upper corner, though the preliminary one was done as mentioned already, then Figs. 6 and 8 will be improved. The energy that the downgoing slab needs to induce the vortex is given by eq. (6). A thermal problem that the mechanical energy changes to heat in the vortex will be discussed in future.

References

1) T. Utsu, Rev. Geophys. Space Phys., **9,** 839 (1971)
2) D.P. McKenzie, Geophys. J. Roy. Astron. Soc., **18,** 1 (1969)
3) N.H. Sleep and M.N. Toksöz, Nature, **33,** 548 (1971)
4) D.J. Andrews and N.H. Sleep, Geophys. J. Roy. Astron. Soc. **38,** 237 (1974)
5) M.N. Toksöz and P. Bird, In: M. Talwani and W.C. Pitman III (Editors), Island Arcs, Deep Sea Trenches and Back-Arc Basins, AGU, Washington, D.C. p. 379 (1977)
6) M.N. Toksöz and A.T. Hsui, Tectonophysics, **50,** 177 (1978)
7) A.T. Hsui and M.N. Toksöz, Tectonophysics, **74,** 89 (1981)
8) M. Kawaguti, J. Phys. Soc. Japan, **16,** 2307 (1961)
9) O. Kinoshita, H. Itô and Y. Masuda, Bull. Univ. Osaka Pref., **A32,** 65 (1983)
10) R.K. McConnell Jr., J. Geophys. Res., **70,** 5171 (1965)
11) R. Geller, Bull. Seism. Soc. Am., **59,** 865 (1976)
12) C.G. Chase, J. Geophys. Res., **83,** 5385 (1978)
13) S. Uyeda and H. Kanamori, J. Geophys. Res., **84,** 1049 (1979)
14) J.B. Minster and T.H. Jordan, J. Geophys. Res., **83,** 5331 (1978)
15) T. Seno, Tectonophysics, **42,** 209 (1977)
16) D.E. Karig, Geol. Soc. Am. Bull., **82,** 323 (1971)
17) D.E. Karig, R.N. Anderson and L.D. Bibee, J. Geophys. Res., **83,** 1213 (1978)
18) X. Le Pichon, J. Francheteau and G.F. Sharman III, J. Phys. Earth, **23,** 251 (1975)
19) D.R. Brancey and T.A. Ogden, Geol. Soc. Am. Bull., **83,** 1509 (1972)
20) D.E. Karig, J. Geophys. Res., **75,** 239 (1970)
21) D.E. Karig, J. Geophys. Res., **76,** 2542 (1971)
22) Y. Katsui (ed.) ,List of the world active volcanoes (with map), Special issue of Bulletin of volcanic eruptions (1971)
23) E.R. Engdahl, N.H. Sleep and M.T. Lin, Tectonophysics, **37,** 95 (1977)
24) T. Yoshii, Kagaku, **47,** 170 (in Japanese) (1977)
25) M. Katsumata and L.R. Sykes, J. Geophys. Res., **74,** 5923 (1969)
26) W. Hamilton, Earthquake map of the Indonesian region, Map I-875-C, U.S. Geol. Surv., Reston, Va. (1974)
27) D. Denham, J. Geophys. Res., **74,** 4290 (1969)
28) J. Dubois, J. Geophys. Res., **76,** 7217 (1971)
29) B.L. Isacks and M. Barazangi, In: M. Talwani and E.C. Pitman III (Editors), Island Arcs, Deep Sea Trenches and Back-Arc Basins, AGU, Washington, D.C., p. 99 (1977)
30) T. Santo, Bull. Earthquake Res. Inst., **48,** 1089 (1970)
31) J.W. Dewey and S.T. Algermissen, Bull. Seism. Soc. Am., **64,** 1033 (1974)